Monatshefte für Chemie - Chemical Monthly
https://doi.org/10.1007/s00706-024-03251-y

ORIGINAL PAPER

Copper(II) oxide-modified screen-printed carbon electrode for electrochemical detection of tuberculosis and mycobacterial infections treating drugs: rifampicin

Shengzhou Qiu[1] · Chenxi Wu[1] · Sima Akter[2] · Shaoli Hong[1] · Huihong Liu[1] · Sakil Mahmud[3]

Received: 25 June 2024 / Accepted: 17 August 2024

Abstract

Addressing the challenges of tuberculosis drug detection, this study investigates the application of copper(II) oxide modified screen-printed carbon electrodes (CuO/SPCEs) for the electrochemical detection of rifampicin, a critical drug in the treatment of tuberculosis and mycobacterial infections. The CuO/SPCE was fabricated via a constant potential electrodeposition technique and characterized using voltammetry. The bare SPCE surface exhibited a rough, porous structure, whereas the electrodeposition of CuO resulted in a smoother CuO/SPCE surface. The sensor exhibited high sensitivity with a detection limit of 2.89 µM for rifampicin and demonstrated excellent stability with a relative standard deviation of 3.5% over 10 measurements. The reproducibility was confirmed with an RSD of 4.2% across different electrodes. It also showed a linear response to rifampicin concentrations ranging from 10 to 200 µM. The real sample analysis showed a linear relationship between rifampicin concentration and peak current ($I = 0.739 + 0.008\ c$), with a high correlation coefficient ($R^2 = 0.995$). This electrochemical sensor's simplicity, cost-effectiveness, and rapid response make it a promising tool for point-of-care applications in tuberculosis management.

Graphical abstract

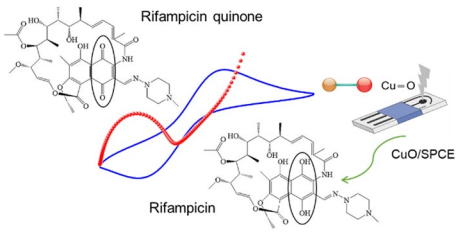

Keywords Electrochemical sensor · CuO-modified electrode · Rifampicin detection · Tuberculosis · Screen-printed carbon electrode

✉ Huihong Liu
huihongliu@wtu.edu.cn

✉ Sakil Mahmud
smahmud@lincoln.edu

[1] College of Chemistry and Chemical Engineering, Hubei Key Laboratory of Biomass Fibers and Eco-Dyeing & Finishing, Wuhan Textile University, Wuhan 430200, People's Republic of China

[2] Enam Medical College and Hospital, Faculty of Medicine, University of Dhaka, Dhaka 1000, People's Republic of Bangladesh

[3] Department of Chemistry and Physics, Lincoln University, 1570 Baltimore Pike, Oxford, PA 19352, USA

Published online: 09 September 2024

Introduction

Tuberculosis (TB) remains a major global health challenge, accounting for significant morbidity and mortality worldwide [1]. The World Health Organization (WHO) estimates that TB is responsible for over 1.5 million deaths annually, making it one of the leading causes of death from infectious diseases [2]. Despite extensive efforts to control the disease, the emergence of multidrug-resistant (MDR) and extensively drug-resistant (XDR) strains of *Mycobacterium tuberculosis* has compounded the difficulty of TB treatment and control [3]. Rifampicin (RIF) is a cornerstone in the treatment regimen for TB due to its potent bactericidal activity against *Mycobacterium tuberculosis* [4]. It functions by inhibiting DNA-dependent RNA polymerase, thus blocking RNA synthesis and leading to bacterial cell death [5].

The reliable detection and quantification of RIF in biological samples are crucial for effective TB management, ensuring proper dosing, monitoring therapeutic levels, and detecting potential drug resistance [6]. Traditional methods for the detection of RIF and similar drugs include high-performance liquid chromatography (HPLC), mass spectrometry (MS), and UV–Vis spectrophotometry [7]. HPLC offers high accuracy and sensitivity [8] but requires sophisticated instrumentation and extensive sample preparation. MS provides precise molecular identification [9] but is costly and demands specialized skills. UV–Vis spectrophotometry is relatively simple and cost-effective [10], yet it lacks the sensitivity and specificity needed for complex biological matrices. These methods, despite their advantages in accuracy and precision, are limited by their need for expensive equipment, extensive sample handling, and the inability to provide rapid, on-site analysis, making them less practical for routine monitoring and point-of-care applications [7, 11].

Electrochemical sensing has emerged as a promising alternative due to its inherent advantages, including high sensitivity, rapid response, low cost, and the capability for miniaturization [12]. Electrochemical sensors, particularly those based on modified electrodes, have been widely studied for detecting various analytes, including pharmaceuticals [13, 14]. Among the various electrode materials, carbon-based electrodes such as screen-printed carbon electrodes (SPCEs) have gained significant attention in the detection of RIF and similar drugs due to their unique advantages over traditional methods [15, 16]. SPCEs offer a cost-effective, disposable, and user-friendly platform for electrochemical sensing, enabling rapid and on-site analysis without the need for extensive sample preparation or expensive instrumentation. Previous reports have demonstrated the efficacy of SPCEs in detecting various pharmaceuticals, highlighting their high sensitivity, selectivity, and reproducibility [17]. For instance, modified SPCEs have been successfully used to detect paracetamol [18, 19], isoniazid [20], and pyrazinamide [21], showing excellent performance in terms of detection limits and linearity ranges.

Various nanomaterials have been employed to modify SPCEs for enhanced electrochemical detection of drugs, each with distinct advantages and drawbacks [20]. Noble metals like gold, silver, and platinum nanoparticles provide excellent conductivity and catalytic activity, significantly boosting sensor sensitivity and selectivity [22]. However, their high cost and potential for aggregation limit their practicality for widespread use. Carbon-based nanomaterials, such as graphene and carbon nanotubes, offer large surface areas and remarkable electronic properties, improving detection limits and response times [15, 23]. Despite these benefits, issues like poor dispersion and complex synthesis processes hinder their scalability. Metal oxides, including ZnO, iron(III) oxide, and TiO_2, present an attractive balance of cost and performance [24, 25], but their electrochemical activity can be inconsistent and heavily dependent on synthesis conditions. Thus, while these nanomaterials bring valuable improvements, their limitations necessitate further exploration for more practical alternatives.

Copper(II) oxide (CuO) stands out as a superior modifier for SPCEs due to its unique properties and advantages over other nanomaterials [26]. CuO offers excellent electrochemical activity, high surface area, and good stability, which are crucial for enhancing the sensitivity and selectivity of the sensor [26]. Unlike noble metals, CuO is cost-effective, making it more suitable for large-scale applications and disposable sensors [27]. It's simple synthesis and compatibility with various substrates further enhance its appeal for practical use [28]. CuO-modified SPCEs have demonstrated remarkable performance in detecting drugs and biological macromolecules, with improved detection limits and linearity compared to other modifiers [26, 29]. CuO's catalytic properties also facilitate efficient electron transfer and redox reactions, which are critical for accurate and rapid electrochemical sensing [30]. These advantages make CuO a promising and versatile choice for developing advanced electrochemicals. Interestingly, these features of CuO for the modification of SPCE have not been explored for the detection of tuberculosis and mycobacterial infection treatment drugs like RIF. Of course, there are some relevant reports where the process and ultimate objectives differ. For example, Dhara et al. [31] synthesized a Pd-CuO/rGO nanocomposite for a nonenzymatic glucose sensor, achieving high sensitivity (3355 μA mM^{-1} cm^{-2}) and low detection limit (30 nM). Tajik et al. [30] developed a Fe_3O_4/CuO nanoparticle-modified electrode for desipramine detection with a wide linear range (0.08–400.0 μM). Choudhry et al.

[32] created a CuO-modified electrode with high selectivity and a glucose detection limit of 0.06 µM. Liu et al. [33] reported a CuO/MWCNTs-modified electrode for glucose sensing with high electrocatalytic activity and a detection limit of 4 µM.

In this study, we developed a CuO-modified screen-printed carbon electrode (CuO/SPCE) for the electrochemical detection of RIF. The choice of CuO as a modifying agent is motivated by its excellent electron transfer capabilities and catalytic activity enhancement. The modification process involves electrodeposition of CuO onto the SPCE, followed by voltammetry characterization. The electrochemical behavior of RIF at the CuO/SPCE was systematically investigated, optimizing parameters such as $CuSO_4$ concentration, electrodeposition time, scan rate, and pH. Voltametric studies revealed significantly enhanced peak currents for RIF oxidation at CuO/SPCE compared to bare and activated SPCEs, indicating improved sensitivity due to CuO. Furthermore, the effect of scan rate on the electrochemical response showed a linear relationship between peak current and scan rate, suggesting a surface-controlled process. The influence of pH on RIF's electrochemical behavior indicated a proton-coupled electron transfer mechanism. The CuO/SPCE demonstrated excellent analytical performance, making it a reliable, sensitive, and efficient method for RIF detection in pharmaceutical formulations.

Results and discussion

Modification and characterization of electrodes

In optimizing the electrodeposition of CuO on SPCE for the electrochemical detection of RIF, different concentrations of $CuSO_4$ (ranging from 10^{-6} to 10^{-3} M) were explored in PBS at pH 7 (Fig. 1a_1–a_2). The electrodeposition was conducted at a constant potential of +1.6 V, and cyclic voltammetry (CV) was recorded at a scan rate of 50 mV/s. The results indicate a nuanced relationship between $CuSO_4$ concentration and the electrochemical performance of the CuO-modified electrodes. As the concentration of $CuSO_4$ increased from 10^{-6} to 10^{-4} M, the peak current (*I*) also increased, reaching a maximum value at 10^{-4} M (3.989 µA). This suggests an enhancement in the electroactive surface area and the conductivity of the CuO layer, which may facilitate electron transfer during the detection of RIF. However, at a concentration of 10^{-3} M, the peak current decreased to 3.077 µA. This decrease can be attributed to forming a thicker and possibly less conductive CuO layer, which may hinder the diffusion of the analyte (RIF) to the electrode surface. Therefore, the optimal concentration of $CuSO_4$ for electrodeposition was determined to be 10^{-4} M, balancing the surface coverage and conductivity of the CuO layer. Using a lower concentration of $CuSO_4$, the electrodeposition medium can be either a natural or alkaline solution, allowing CuO to be easily deposited on the surface of the SPCE and form as isolated single molecules or nanoclusters.

The effect of electrodeposition time on the performance of CuO-modified SPCE was also studied (Fig. 1b_1–b_2). Electrodeposition times ranged from 20 to 100 s at a constant potential of +1.6 V, with subsequent CV measurements recorded for 100 µM RIF in 0.1 M PBS at pH 7. The electrodeposition time significantly influences the formation and effectiveness of the CuO layer on the SPCE. The peak current initially increased with the electrodeposition time, reaching a maximum of 40 s (3.219 µA). This suggests that an optimal deposition time enhances the electroactive surface area and improves the sensor's performance. However, beyond 40 s, the peak current decreased, indicating that longer deposition times result in a thicker CuO layer, which can impede the diffusion of RIF to the electrode surface. This thicker layer likely presents a higher resistance to electron transfer, thereby reducing the overall electrochemical response.

In summary, the optimal conditions for the electrodeposition of CuO on SPCE were determined based on the effects of $CuSO_4$ concentration and electrodeposition time. A concentration of 10^{-4} M $CuSO_4$ and an electrodeposition time of 40 s were found to be the most effective, yielding the highest peak currents and, therefore, the best electrochemical performance for detecting RIF. These findings provide crucial insights into preparing CuO-modified electrodes, ensuring high sensitivity and reliability in electrochemical sensing applications.

To investigate the electrochemical behavior of electrodes, it has been focused on the redox dynamics at various modification stages. Figure 1c compares CV analyses for bare SPCE, active SPCE, and CuO/SPCE using 0.5 mM $K_3[Fe(CN)_6]$ in 0.1 M PBS at pH 7 with a scan rate of 50 mV/s. The activation of SPCE resulted in higher peak currents, reflecting an improved electrochemical response. In contrast, CuO modification led to a slight decrease in oxidation peak current compared to the active SPCE, although it remained higher than that of the bare SPCE, suggesting a surface-controlled mechanism for reactants at the electrode surface [34]. The bare SPCE displayed an oxidation peak at 0.454 V with a current of 2.3 µA and no reduction peak, indicating slow electron transfer likely due to insulating additives in the conductive inks [35]. Activating the SPCE produced a clear oxidation peak at 0.232 V with a current of 7.5 µA and a reduction peak at −0.015 V with a current of −6.8 µA, indicating improved electron transfer kinetics [36]. CuO/SPCE showed further enhanced electron transfer kinetics, with an oxidation peak at 0.252 V and a current of 5.5 µA and a reduction peak at −0.042 V and a current of −7.9 µA. This indicates reduced peak potential

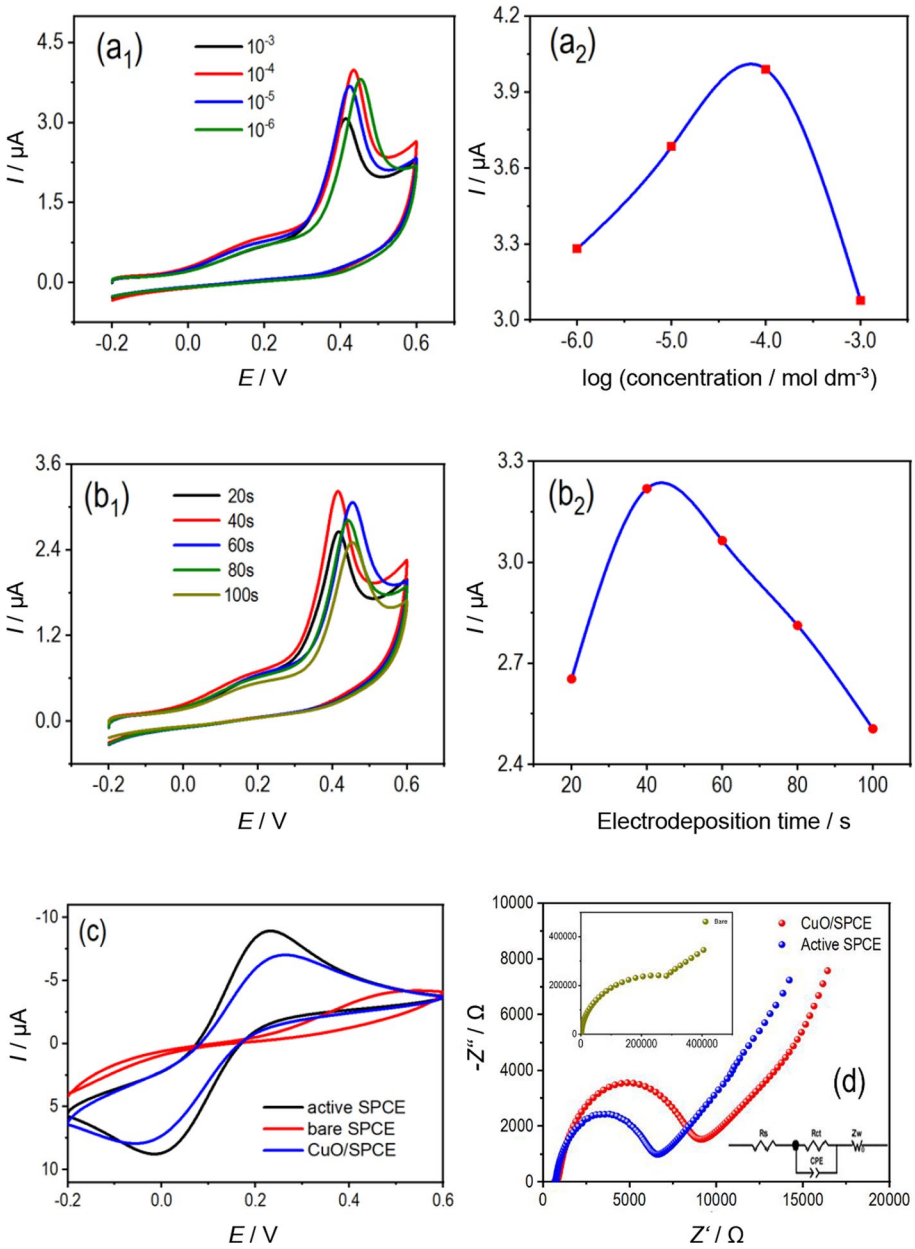

Fig. 1 CVs of SPCE were obtained under varying conditions: $\mathbf{a_1}$ different concentrations of $CuSO_4$, $\mathbf{b_1}$ varying electrodeposition times, and $\mathbf{a_1}$–$\mathbf{b_2}$ their respective anodic current plots (CVs recorded in 0.1 M PBS/ pH = 7 with a scan rate of 50 mV/s). **c** CVs (recorded in 0.1 M PBS/ pH = 7 with a scan rate of 50 mV/s) and **d** electrochemical impedances are recorded at bare SPCE, active SPCE, and CuO/SPCE (recorded in 0.1 M PBS/ pH = 7 with a scan rate of 50 mV/s, frequency: 100,000–0.01 Hz, and amplitude: 10 mV RMS), with their corresponding circuit diagram (lower inset). All corresponding data are shown in Table S1–S3

separation and increased peak currents compared to bare SPCE, confirming the successful immobilization of CuO on the SPCE surface and its role in enhancing electrochemical performance. These findings collectively show that both activation and CuO modification significantly improve the electrochemical response of SPCE, with the CuO/SPCE exhibiting enhanced redox behavior due to superior electron transfer kinetics and a larger electroactive surface area.

Electrochemical impedance spectroscopy (EIS) is a crucial method for investigating the interfacial properties between the electrolyte solution and various sensing interfaces. The Nyquist plot derived from EIS typically includes a high-frequency elliptical representing the charge transfer resistance (R_{ct}) and a low-frequency linear part indicative of surface-controlled processes. In Fig. 1d, the Nyquist plot illustrates the impedance data for different configurations of SPCE: bare SPCE, activated SPCE, and CuO/SPCE. The measurements were conducted using a redox probe, $Fe(CN)_6^{3-/4-}$, in a solution of 0.5 mM $K_3[Fe(CN)_6]$ in 0.1 M PBS at pH 7. The scan rate was set at 50 mV/s, with a frequency range from 100 kHz to 0.01 Hz and an amplitude of 10 mV RMS. The Nyquist plots determined the R_{ct} values: 4777.870 kΩ for bare SPCE, 5.031 kΩ for activated SPCE, and 6.584 kΩ for CuO/SPCE. The significant reduction in R_{ct} values for both active SPCE and CuO/SPCE compared to the bare SPCE indicates enhanced conductivity and improved electrochemical activity [37]. Specifically, the lower R_{ct} value for CuO/SPCE compared to

bare SPCE suggests a more efficient charge transfer process. This improvement is due to the presence of CuO, which enhances electron transfer at the electrode interface, thereby improving the overall electron-transfer kinetics. Adekunle et al. [38] observed similar results in their study on the electrochemical behavior of dopamine and epinephrine using a platinum electrode modified with a carbon nanotubes-gold nanocomposite.

The electrode surface morphology was examined using SEM before and after electrochemical pretreatments (Fig. 2a_1 and b_1). The bare SPCE surface displayed a rough structure with large pores, multilayers, and a sponge-like network with nano-size cavities (Fig. 2a_1). In contrast, the CuO/SPCE surface was smoother (Fig. 2b_1). Electrochemical treatment with CuO significantly smoothed the bare SPCE surface, indicating that electrochemical activation

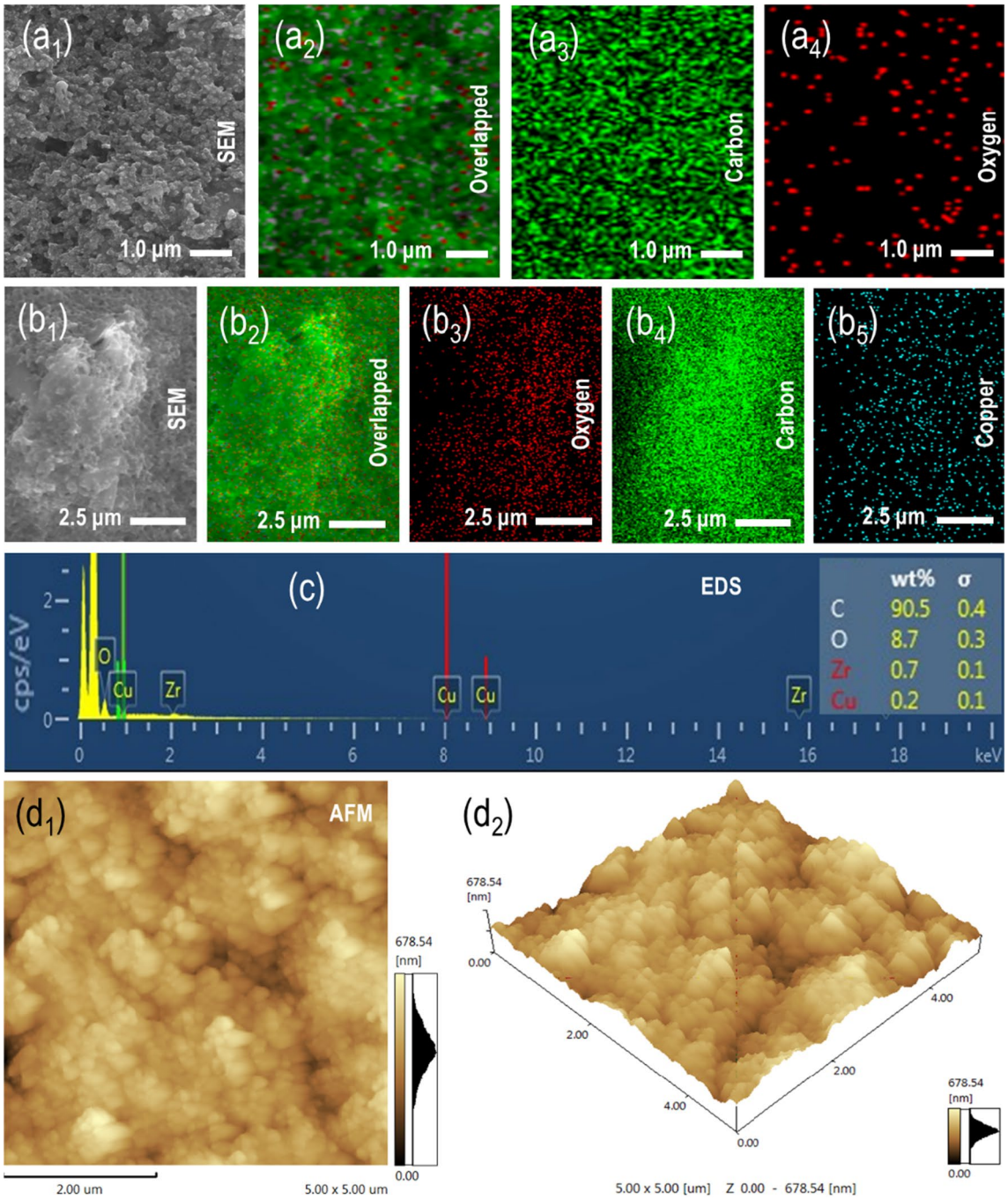

Fig. 2 SEM images with their corresponding elemental mapping of $\mathbf{a_1}$–$\mathbf{a_4}$ bare SPCE and $\mathbf{b_1}$–$\mathbf{b_5}$ CuO/SPCE. EDX spectrum of **c** and AFM mages $\mathbf{c_1}$–$\mathbf{c_2}$ of CuO/SPCE

profoundly alters surface morphology, enhancing its electrochemical sensor characteristics. EDX (Fig. 2c) and elemental mapping (Fig. 2a_2–a_4 and b_2–b_5) confirmed the uniform distribution of Cu. AFM analysis revealed a significantly different topography post-CuO modification, with a height of 678.54 nm and an average roughness of 80.63 nm (Fig. 2d_1–d_2).

The chemical valence states of the primary elements C, O, and Cu in the CuO/SPCE were investigated using X-ray photoelectron spectroscopy (XPS). The survey XPS spectrum indicates the presence of C (284.8 eV), O (532.1 eV), and Cu (934.6 eV) on the surface of the CuO/SPCE (Fig. 3a). In the high-resolution spectra of C 1 s (Fig. 3b), four characteristic peaks are observed at binding energies of 284.8, 286.4, 287.6, and 288.9 eV, suggesting the presence of various carbon oxidation states. The peak at 284.8 eV corresponds to C=C bonds, the peak at 286.4 eV corresponds to C–O bonds, the peak at 287.6 eV corresponds to C=O bonds, and the peak at 288.9 eV corresponds to O–C=O bonds [39]. The high-resolution spectra of O 1 s (Fig. 3c) exhibit peaks at 532.1 and 533.1 eV, which can be attributed to Cu–O and O–C bonds, respectively [40]. The high-resolution spectra of Cu 2p (Fig. 3d) provide further insights into the chemical state of copper. The Cu $2p_{3/2}$ and Cu $2p_{1/2}$ doublets observed at 934.6 and 954.2 eV, respectively, indicate Cu^{2+} oxidation states [41]. Additionally, the satellite peaks at 940.7, 943.9, and 944.6 eV further confirm the presence of Cu^{2+} ions [42]. These results collectively demonstrate that the modifier electrodeposited on SPCE primarily consists of CuO.

Electrochemical behaviors of RIF at CuO/SPCE

The CVs of RIF recorded at bare SPCE, active SPCE, and CuO/SPCE demonstrate significant enhancements in both peak current and peak potential for RIF oxidation. As shown in Fig. 4a, the peak current (*I*) for RIF oxidation at CuO/SPCE (2.574 µA) is substantially higher than that at bare SPCE (0.5575 µA) and active SPCE (1.999 µA), indicating a marked improvement in electrochemical response due to the modification with CuO. Additionally, the oxidation peak potential (*E*) at CuO/SPCE (0.475 V) is slightly lower than that at active SPCE (0.486 V) but higher than that at bare SPCE (0.191 V), suggesting that CuO facilitates electron transfer and enhances the electrochemical activity of RIF. The negative shift of the oxidation peak potential indicates the catalysis of CuO to RIF. The lowest potential was observed at bare SPCE (0.191 V), possibly due to the catalysis of organic molecules and additives in the ink used for preparing SPCE. This phenomenon can be attributed to the increased surface area, better conductivity, and catalytic properties of metal oxide nanoparticles, which provide more active sites for the electrochemical reaction [43]. Herein,

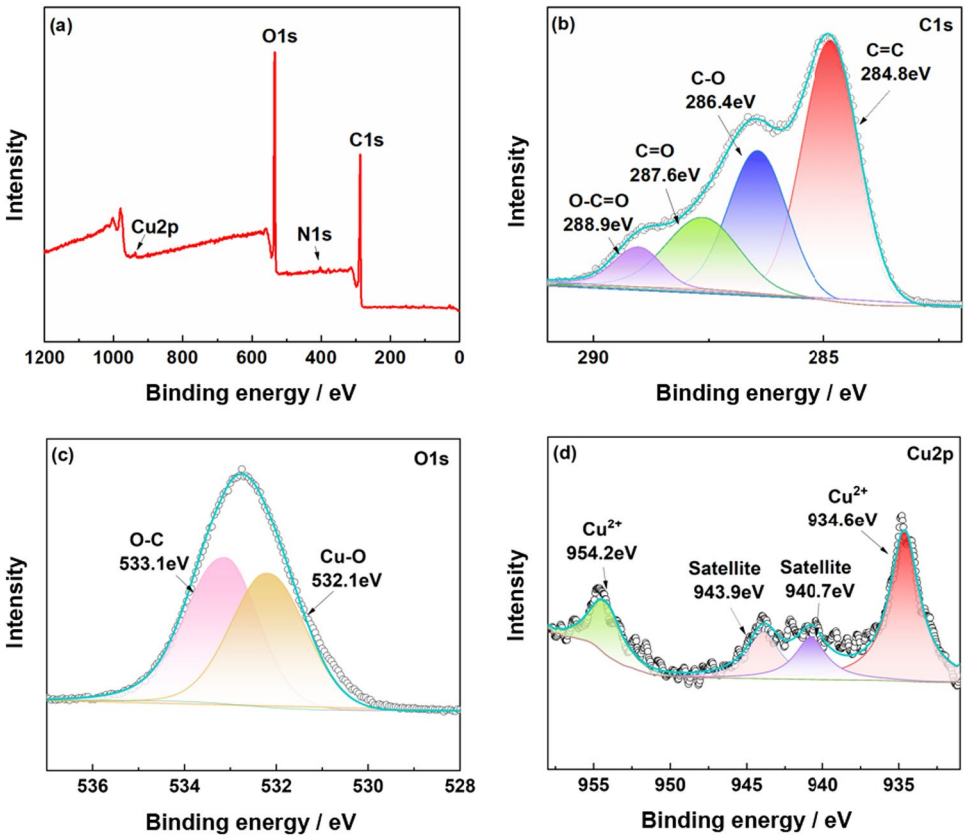

Fig. 3 XPS spectrum of CuO/SPCE: **a** Survey and high-resolution spectra of **b** C 1 s, **c** O 1 s, and **d** Cu 2p

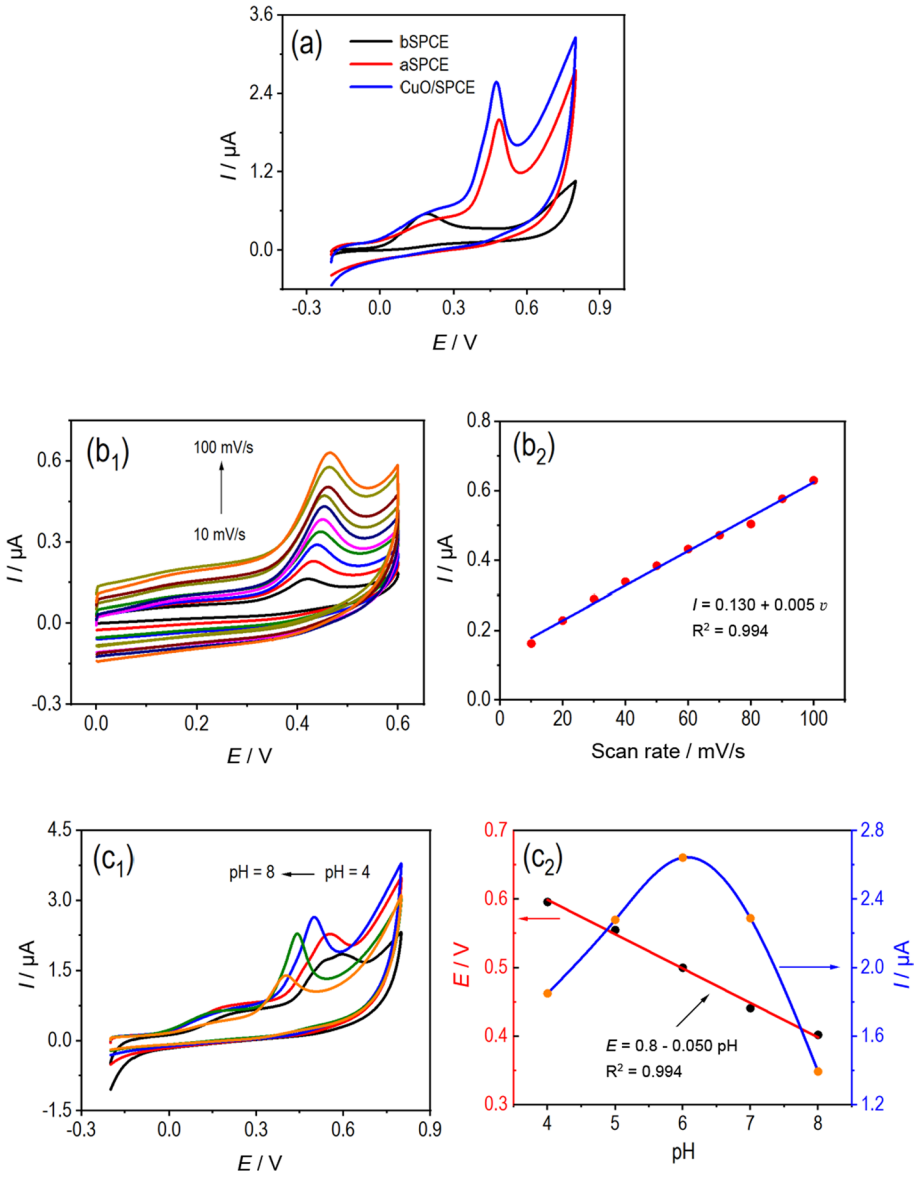

Fig. 4 **a** CVs of RIF (100 µM) recorded at SPCE, aSPCE, and CuO/SPCE (0.1 M PBS, pH = 7 and scan rate: 50 mV/s). $\mathbf{b_1}$ CVs of INZ (10 µM) recorded at CuO/SPCE at different scan rates (0.1 M PBS/ pH = 7), and $\mathbf{b_2}$ the corresponding plots of anodic peak currents versus the scan rates. $\mathbf{c_1}$–$\mathbf{c_2}$ CVs of RIF recorded at CuO/SPCE at different pH levels and their respective plots of anodic peak currents (0.1 M PBS and scan rate: 50 mV/s). All corresponding data are tabulated in Table S4–S6

Scheme 1

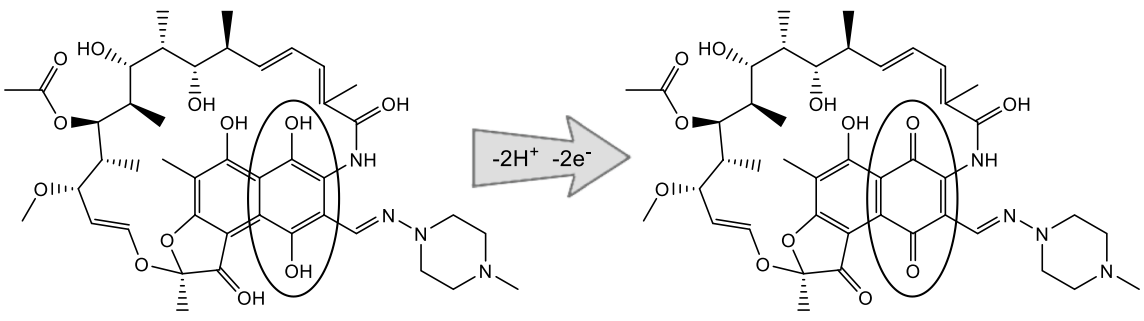

Rifampicin Rifampicin quinone

hydrogen bonds in the hydroxyl groups of RIF are broken, releasing two electrons and resulting in the oxidation of RIF to RIF quinone via CuO nanoparticles [44] (Scheme 1).

The CVs of RIF at CuO/SPCE were recorded at various scan rates (10–100 mV/s) to investigate the effect of scan rate on the electrochemical behavior. As indicated in Fig. 4b_1–b_2, the peak current increases linearly with the scan rate, suggesting an adsorption-controlled electrochemical process. The linear relationship is given by $I = 0.130 + 0.005\ \upsilon$ with an R^2 value of 0.994, indicating excellent correlation. This implies that the oxidation of RIF at CuO/SPCE is primarily governed by the diffusion of RIF molecules to the electrode surface, which is typical for many electrochemical reactions. The linearity of the plot of peak current (I) versus the scan rate confirms the adsorption-controlled nature of the process, consistent with the Randles–Sevcik equation [45].

The influence of pH on the electrochemical behavior of RIF at CuO/SPCE was studied by recording CVs at different pH values (4–8). As shown in Fig. 4c_1–c_2, the oxidation peak potential (E) shifts negatively with increasing pH, while the peak current (I) initially increases, reaching a maximum at pH 6, and then decreases. The linear relationship between peak potential and pH is described by $E = 0.8–0.050$ pH with an R^2 value of 0.994, indicating a predictable and consistent shift in peak potential with changes in pH. This behavior suggests that protons participate in the oxidation process of RIF, and the reaction becomes easier (less positive potential) as the pH increases due to the decreasing concentration of protons. The peak current behavior, with a maximum at pH 6, suggests that at this pH, the RIF is in its most favorable electrochemical form for oxidation at the CuO/SPCE, likely due to optimal proton availability and species stability.

Based on our understanding, the observed enhancements in the electrochemical response of RIF at CuO/SPCE compared to bare SPCE and active SPCE highlight the significant role of CuO modification in improving the sensitivity and efficiency of the electrode. (a) The increased peak current and favorable shift in peak potential at CuO/SPCE can be attributed to the catalytic properties of CuO nanoparticles, which enhance electron transfer kinetics and provide a larger surface area for the electrochemical reaction. (b) The adsorption-controlled nature of the oxidation process, as indicated by the linear relationship with the scan rate, suggests that mass transport is a critical factor in the electrochemical behavior of RIF at CuO/SPCE. (c) The effect of pH on the electrochemical behavior indicates that the protonation state of RIF and the availability of protons in the solution significantly influence the oxidation process. The negative shift in peak potential with increasing pH and the peak current maximum at pH 6 suggest that the optimal electrochemical detection of RIF occurs under slightly acidic to neutral conditions. This finding is crucial for optimizing the conditions for the electrochemical detection of RIF, ensuring maximum sensitivity and accuracy.

The electrochemical detection of RIF using CuO/SPCE involves a series of electrochemical reactions facilitated by the catalytic properties of CuO nanoparticles. The CuO modification enhances the electron transfer kinetics and increases the surface area, which collectively improves the sensitivity and efficiency of the detection process. The mechanism can be explained through the following aspects: (1) CuO nanoparticles are electrodeposited onto the surface of SPCE, increasing the active surface area and introducing catalytic sites that facilitate the electron transfer process. The CuO nanoparticles are known for their excellent electrocatalytic properties, which enhance the oxidation of RIF. (2) The primary electrochemical detection of RIF at the CuO/SPCE is the oxidation of RIF molecules (Eq. 1). This reaction involves the transfer of an electron from the RIF molecule to the electrode surface, resulting in the formation of an oxidized RIF species (RIF^+). (3) CuO nanoparticles on the electrode surface act as catalytic centers, facilitating the electron transfer from RIF to the electrode. The catalytic mechanism of CuO can be attributed to its ability to mediate redox reactions (Eqs. 2–3). This redox cycle enhances the electron transfer process, making the oxidation of RIF more efficient. (4) The electrochemical behavior of RIF is pH–pH-dependent, as indicated by the shift in peak potential with varying pH. The reaction is facilitated in slightly acidic to neutral conditions, where the proton availability is optimal for the oxidation process (Eq. 4). At lower pH, the higher concentration of protons (H^+) supports the oxidation process, while at higher pH, the reduced proton concentration slows down the reaction. (5) The linear increase in peak current with the scan rate indicates that the oxidation of RIF at CuO/SPCE is a surface-controlled process. This means that the electrochemical reaction rate is determined by the diffusion of RIF molecules to the electrode surface. In summary, RIF undergoes redox reactions on CuO/SPCEs, where CuO significantly enhances the electrochemical detection. The redox mechanism involves the reduction of RIF to its reduced form and its subsequent oxidation back to the original state, facilitated by the catalytic properties of CuO. The CuO modification improves electron transfer kinetics and increases the detection sensitivity by providing active sites for the reactions. This results in well-defined electrochemical peaks, enhanced current response, and better overall reproducibility and stability of the detection process. It highlights the significant role of CuO in improving the electrochemical detection of RIF, making CuO/SPCE a susceptible and efficient platform for analytical applications.

$$RIF \rightarrow RIF^+ + e^- \quad (1)$$

$$CuO(Cu(II)) + e^- \rightarrow Cu_2O(Cu(I)) + O^{2-} \quad (2)$$

$$Cu_2O(Cu(I)) + H_2O \rightarrow 2CuO(Cu(II)) + 2H^+ + 2e^- \quad (3)$$

$$RIF + H_2O \rightarrow RIF^+ + 2H^+ + 2e^- \quad (4)$$

Analytical performance of CuO/SPCE

Electrochemical detection of RIF

The electrochemical detection of RIF using CuO/SPCE was investigated, focusing on determining the analytical performance, including sensitivity, linear response range, and detection limit. DPV was employed to assess the electrochemical behavior of RIF at various concentrations ranging from 10 to 200 µM on CuO/SPCE in 0.1 M PBS at pH 6 (Fig. 5a_1–a_2). The resulting current values were recorded and analyzed. The data presented in Table S7 illustrates the relationship between RIF concentration and the corresponding current response. The calibration curve obtained from the DPV measurements revealed a linear relationship between RIF concentration and peak current, described by the equation $I = 0.972 + 0.005\ c$, with a high correlation coefficient ($R^2 = 0.990$). This linear response range indicates the sensitivity of the CuO/SPCE for RIF detection.

Furthermore, the limit of detection (LoD) was calculated using the standard equation LoD = 3 s/m, where s is the standard deviation of the response and m is the slope of the calibration curve. Based on the obtained linear equation, the calculated LoD was 2.89 µM. This value signifies the lowest concentration of RIF that can be reliably detected using the CuO/SPCE platform. The exceptional performance of CuO/SPCE in electrochemically detecting RIF highlights its potential as a reliable tool for quantitative analysis in real samples. The sensitivity, wide linear range, and low detection limit demonstrate the efficacy and applicability of CuO/SPCE for precise RIF quantification. Moreover, the consistency of the results obtained across different concentrations of RIF underscores the reliability and robustness of the CuO/SPCE platform for electrochemical detection applications. This study provides valuable insights into the electrochemical behavior of RIF and the performance of CuO/SPCE, contributing to advancing electroanalytical techniques for pharmaceutical analysis and related fields.

Stability and reproducibility

The application of SPCEs in electroanalytical chemistry is highly favored due to their affordability, disposability, and

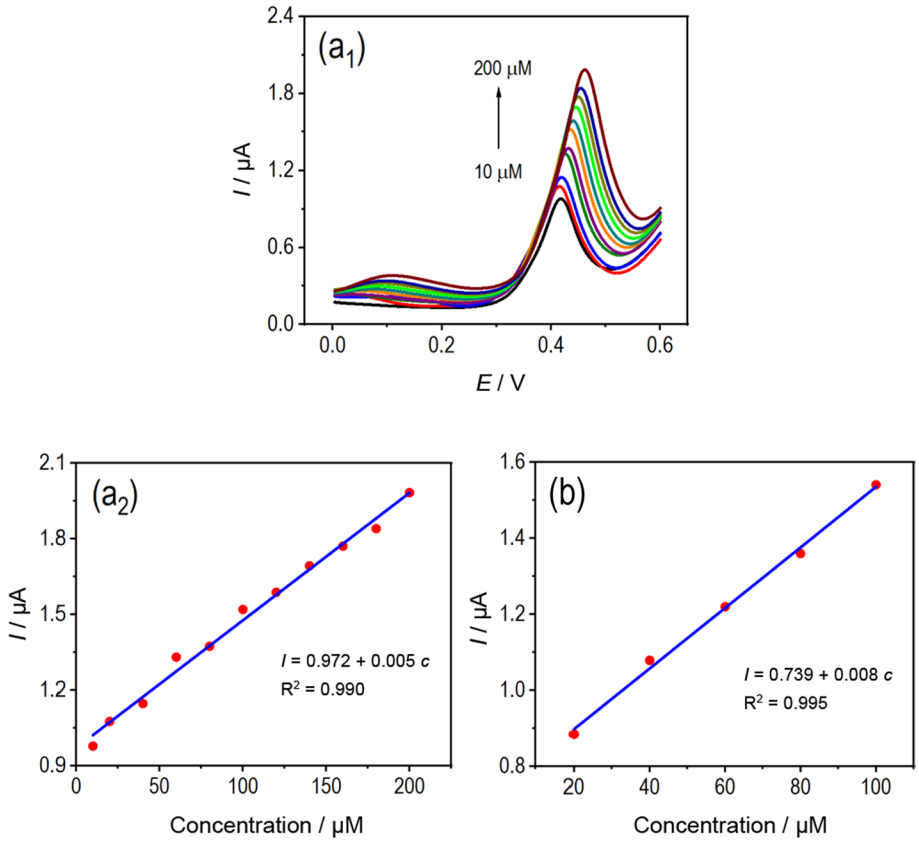

Fig. 5 **a_1** LSVs (0.1 M PBS/pH = 6) of CuO/SPCE at various RIF concentrations and **a_2** their calibration curves. **b** DPVs (0.1 M PBS/pH = 6) of CuO/SPCE at different RIF concentrations, recorded using the standard addition method. All corresponding data are shown in Tables S7, S9, and S10

reliability. However, achieving consistent stability and reproducibility continues to be a critical challenge. Modifying SPCEs with CuO addresses these issues, providing a robust platform for the electrochemical detection of RIF. Seven successive measurements were conducted to assess the stability of the CuO/SPCE (Table S8a–b). The results demonstrated excellent stability with minimal variation in both potential and current. The measured potential values yielded a relative standard deviation (RSD) of 0.58%, while the current measurements resulted in an RSD of 4.00%. These RSD values confirm the electrode's robustness for repeated measurements, indicating that the CuO/SPCE maintains consistent performance across multiple uses. This highlights its reliability for continuous monitoring of RIF.

The reproducibility of the CuO/SPCE was assessed using five individually prepared electrodes to measure RIF (Table S8). The potential values showed an RSD of 0.57%, while the corresponding current measurements resulted in an RSD of 4.22%. These reproducibility assessments, with RSD values of different electrodes, underscore the consistency and reliability of the CuO/SPCE platform. These outcomes suggest that the CuO/SPCE provides highly reproducible results when different electrodes are employed, ensuring the reliability of the method across various samples and conditions. Given these findings, the CuO/SPCE proves to be a reliable tool for the electrochemical detection of RIF, overcoming previous challenges of stability and reproducibility in SPCE-based sensors. This advancement ensures that the CuO/SPCE can be confidently employed in practical applications where precise and dependable measurements are essential.

Interference study

The selectivity of CuO/SPCE for the electrochemical detection of RIF was comprehensively examined to evaluate its applicability in real sample analysis. Various potential interfering species commonly found in pharmaceutical samples were investigated to assess their impact on RIF detection using DPV. Inorganic ions, including CO_3^{2-}, SO_4^{2-}, PO_4^{3-}, Ca^{2+}, K^+, and Na^+, along with glucose and sucrose at 50 times their typical concentrations and vitamin C at 20 times, were examined for their interference with RIF detection. Dopamine and uric acid were evaluated at 10 times their usual concentrations. The findings indicate that none of the tested interfering species caused significant interference (defined as <5% deviation) in the electrochemical detection of RIF. This robust selectivity profile suggests that CuO/SPCE is highly specific to RIF and can effectively distinguish it from various potential interferents commonly encountered in pharmaceutical matrices.

These results are consistent with previous interference studies conducted on similar electrochemical platforms for other analytes [46], validating the reliability and applicability of CuO/SPCE in practical analytical settings. The negligible interference observed underscores the potential of CuO/SPCE as a reliable tool for the sensitive and selective detection of RIF in complex sample matrices. The absence of interference from common interfering species at elevated concentrations further highlights the suitability of CuO/SPCE for pharmaceutical analysis, where accurate and selective detection of RIF is paramount. These findings support using CuO/SPCE as a promising platform for electrochemical RIF detection in pharmaceutical formulations and biological samples, facilitating precise and reliable analysis in diverse analytical settings.

Real sample analysis

The practical utility of CuO/SPCE for the electrochemical detection of RIF in pharmaceutical tablet samples was investigated using the standard addition method. This approach enabled the quantification of RIF within authentic pharmaceutical formulations, mimicking real-world scenarios. DPV was employed to record the current responses of CuO/SPCE at different concentrations of RIF, ranging from 20 to 100 μM, in 0.1 M PBS at pH 6 (Fig. 5c). The resulting DPVs provided valuable insights into the electrochemical behavior of RIF on CuO/SPCE. To validate detection accuracy in real samples, pharmaceutical tablet samples containing RIF were analyzed (Tables S9, S10). The labeled and found values of RIF per tablet were determined to be 0.15 and 0.139 g, respectively, indicating a slight deviation. However, the electrochemical analysis revealed a linear relationship between RIF concentration and peak current, described by the equation $I = 0.739 + 0.008\ c$, with a high correlation coefficient ($R^2 = 0.995$).

The standard addition method was employed to quantify RIF in the pharmaceutical tablet samples. The expected concentrations of RIF in the tablets were determined based on the labeled values, and the recovered concentrations were calculated from the electrochemical measurements. The recovery rates ranged from 91.06 to 106.25%, indicating good agreement between the expected and found values. These results suggest that CuO/SPCE provides reliable and accurate quantification of RIF in pharmaceutical samples. Despite the slight deviation in labeled values, the observed recovery rates underscore the practical relevance and efficacy of CuO/SPCE for real sample analysis. The ability to accurately quantify RIF in pharmaceutical formulations highlights the potential of CuO/SPCE as a valuable tool for pharmaceutical quality control and assurance. Furthermore, the high recovery rates demonstrate the robustness and reliability of the developed electrochemical sensing platform in practical analytical applications. The overall analytical

performance of different electrodes for RIF detection is tabulated in Table 1 and compared, indicating the comparable performance of CuO/SPCE.

Conclusion

In this study, we present the development of CuO-modified SPCEs that demonstrate exceptional performance in the sensitive and rapid detection of RIF. Introducing CuO to the SPCE surface, which initially possessed a rough, porous texture, resulted in a significantly smoother electrode surface. The CuO-modified electrodes achieved a remarkable detection limit of 2.89 µM, exhibited high reproducibility with an RSD of 4.2% across different electrodes, and maintained excellent stability with an RSD of 3.5% over ten measurements. Analysis of real samples revealed a strong linear correlation between RIF concentration and peak current ($I = 0.739 + 0.008\ c$), with a high correlation coefficient ($R^2 = 0.995$). These attributes underscore the sensor's effectiveness for monitoring RIF levels in biological samples. The development of this sensor represents a significant advancement in providing a reliable, cost-effective, and user-friendly method for drug detection, which could enhance TB treatment management. Future research will focus on extending the sensor's application to other TB medications and evaluating its performance in clinical settings.

Experimental

Uric acid, sucrose, glucose, dopamine, and ascorbic acid were sourced from Aladdin, China. Copper(II) sulfate ($CuSO_4$), potassium ferricyanide ($K_3Fe(CN)_6$), potassium chloride (KCl), potassium nitrate (KNO_3), sodium hydroxide (NaOH), potassium dihydrogen phosphate dihydrate ($KH_2PO_4{\cdot}2H_2O$), and disodium hydrogen phosphate dodecahydrate ($Na_2HPO_4{\cdot}12H_2O$) were procured from Sinopharm Chemical Reagent Co., Ltd., Shanghai, China. Rifampicin (RIF) tablets, each containing 0.15 g of the drug, were obtained from Tian Guangyuan Biotech Co., Ltd., Xi'an, China, through a local pharmacy. Fresh stock solutions of RIF were prepared daily by dissolving the appropriate amount of RIF in water. The working standard solutions were formulated by diluting the stock solutions with 0.1 M phosphate-buffered saline (PBS) at pH 7.0. All chemicals, of analytical reagent grade, were used without further purification, and all solutions were prepared with ultrapure water having a conductivity of $\leq 18.3\ k\Omega\ cm^{-1}$.

Electro modification of SPCE

Following Jin et al.'s method for atom-by-atom electrodeposition of cobalt oxide on carbon fiber for nanoelectrode fabrication [59], CuO-modified SPCEs were prepared using a constant potential technique. The SPCE was submerged in a solution containing 0.1 µM Cu^{2+} dissolved in 0.1 M phosphate buffer at pH 7.0. A constant potential of +1.6 V versus Ag/AgCl was administered to the SPCE surface for

Table 1 Comparison of the analytical performance of different electrodes for RIF detection

Electrodes	Method	Sample	pH	Linear range/µM	LOD/µM	Rep. (RSD)	References
CuO/SPCE	DVP	Tablet	6.0	10–200	2.89	4.2	This Work
$Ni(OH)_2$/RGO/GCE	LSV	Tablet	7.0	0.004–10	0.002	3.5	[47]
Surfactant/CPE	DPV	–	2.0	3.5×10^{-4}–5.4×10^{-3}	0.0001	2.7	[48]
β-Cyclodextrin/Ppyr/Pt	AMP	Tablet	7.0	2.61–25.23	1.69	3.51	[49]
Lead film/GCE	ASV	Capsule	5.0	2.5×10^{-4}–0.01	9×10^{-5}	–	[50]
DyNW/CPE	AdSWV	Human urine and capsules	5.0	1×10^{-5}–0.0075	5×10^{-5}	–	[51]
PVP-capped $CoFe_2O_4$@CdSe/GCE	AdSWV	Tablet and human serum	2.0	1×10^{-10}–10^{-1}	4.5×10^{-11}	2.62	[52]
PMel-Au_{nano}/GCE	LSV	–	7.0	0.08–15.00	0.03	2.8	[53]
PVP-AgNPs/PANSA/EG-CYP2E1	DPV	Serum	2.0	2–14	0.05	–	[54]
Renewable PGE	DPASV	Tablet	2–3	0.019–1.19	0.013	–	[55]
C-dots/$CuFe_2O_4$/CPE	SWV	Biological fluids and tablet	7.0	0.07–8.0	0.022	3.13	[56]
ZrO_2@chitosan/GCE	DPV	Human serum and urine	7.0	0.015–547.4	0.0075	3.76	[57]
CPE	DPASV	Pharmaceutical	8.0	0.033–0.38	6.13	–	[58]

AdSWV Adsorptive square wave voltammetry, *AgNPs* silver nanoparticles, *AMP* Amperometric procedure, *CPE* Carbon paste electrode, *CYP2E1* Cytochrome P450-2E1, *DPASV* differential pulse adsorptive stripping voltammetry, *DyNW* Dysprosium hydroxide nanowires, *EG* Ethylene glycol bis(succinic acid *N*-hydroxysuccinimide ester), *GCE* glassy carbon electrode, *PANSA* poly(8-anilino-1-naphthalene sulfonic acid), *PGE* renewable pencil graphite electrode, *PMel-*Au_{nano} Poly-melamine gold nanoparticle, *Ppyr/Pt* Polypyrrol platinum electrode, *PVP* polyvinylpyrrolidone, *RGO* reduced graphene oxide, *SWAdASV* square-wave adsorptive anodic stripping voltammetry

a duration of 1.0 min. Subsequently, the altered electrode underwent rinsing with water and was subsequently stored in PBS at pH 7.0. This adapted electrode is denoted as CuO/SPCE.

Characterizations and measurements

The SPCEs crafted for this study were produced measuring 4×0.5 cm^2 with a diameter of 2 mm, comprising a carbon working electrode, a silver/silver chloride (Ag/AgCl) reference electrode, and a carbon auxiliary electrode. The bare SPCEs were supplied by the Institute of Environment and Safety, Wuhan Academy of Agricultural Science. Cyclic voltammetry (CV) analyses were performed employing a CHI612D instrument (Chenhua Corp, Shanghai, China), while electrochemical impedance spectra (EIS) were captured using the P3000ADX electrochemical workstation (Princeton Applied Research, USA). Unless noted otherwise, CV and EIS measurements were executed utilizing a 0.1 M potassium chloride (KCl) solution containing 1 mM potassium hexacyanoferrate (III) ($K_3[Fe(CN)_6]$). During CV, the electrode underwent scanning from −0.5 to 0.5 V at a rate of 100 mV/s for 10 cycles. EIS examination was performed in the identical solution across a frequency span from 100 kHz to 0.1 Hz, comprising 10 data points per decade and an amplitude of 0.005 V.

The surface structure of the electrodes was examined employing a JSM 7800F scanning electron microscope (SEM) manufactured by JEOL Ltd., Japan, coupled with an Energy-dispersive X-ray Spectroscopy detector (EDS) provided by Oxford Instruments, headquartered in Abingdon, Oxfordshire, UK. The surface features of the various modified electrodes were assessed utilizing an atomic force microscope (AFM) model SPM-9700, manufactured by Shimadzu Corp., located in Kyoto, Japan. Chemical states were examined via X-ray photoelectron spectroscopy (XPS) employing an AXIS SUPRA apparatus from KRATOS, which was outfitted with an Al Kα X-ray source (with an excitation energy of 1486.6 eV).

Drug preparation and analysis

The rifampicin tablets were first ground finely with an agate mortar and pestle, followed by the transfer of 0.015 g of the resulting powder into a 100 cm^3 flask. Around 10 cm^3 of water was introduced, and the combination was subjected to ultrasonic extraction for 15 min, after which the resulting solution was stored in the refrigerator. The standard addition technique was utilized to evaluate the efficiency of CuO/SPCE in detecting isoniazid in pharmaceuticals. This procedure entailed diluting the samples in supporting electrolytes and fortifying them with varying concentrations of standard rifampicin solutions.

Supplementary Information The online version contains supplementary material available at https://doi.org/10.1007/s00706-024-03251-y.

Acknowledgements The authors express their gratitude for the generous support of this work from the following organizations: [a] National Natural Science Foundation of China (Grant No. 22204123), [b] Natural Science Foundation of Hubei Province (Grant No. 2022CFB1002), and [c] Key Laboratory of Biomass Fibers & EcoDyeing and Finishing, Hubei Province (Grant No. STRZ2022011).

Data availability Not Applicable.

References

1. Chakaya J, Petersen E, Nantanda R, Mungai BN, Migliori GB, Amanullah F, Lungu P, Ntoumi F, Kumarasamy N, Maeurer M, Zumla A (2022) Int J Infect Dis 124:S26
2. Al Abri S, Kasaeva T, Migliori GB, Goletti D, Zenner D, Denholm J, Al Maani A, Cirillo DM, Schön T, Lillebæk T, Al-Jardani A, Go U-Y, Dias HM, Tiberi S, Al Yaquobi F, Khamis FA, Kurup P, Wilson M, Memish Z, Al Maqbali A, Akhtar M, Wejse C, Petersen E (2020) Int J Infect Dis 92:S60
3. Verma AK, Yadav RN, Kumar G, Dewan RK (2022) J Clin Tuberc Other Mycobact Dis 27:100317
4. Asif M, Qusty NF, Alghamdi S (2024) Med Chem 20:268
5. Mosaei H, Zenkin N (2020). EcoSal Plus. https://doi.org/10.1128/ecosalplus.esp-0017-2019
6. Boehme CC, Nabeta P, Hillemann D, Nicol MP, Shenai S, Krapp F, Allen J, Tahirli R, Blakemore R, Rustomjee R, Milovic A, Jones M, O'Brien SM, Persing DH, Ruesch-Gerdes S, Gotuzzo E, Rodrigues C, Alland D, Perkins MD (2010) N Engl J Med 363:1005
7. Kotadiya RM, Patel FN (2021) Current Pharm Anal 17:983
8. Louveau B, Fernandez C, Zahr N, Sauvageon-Martre H, Maslanka P, Faure P, Mourah S, Goldwirt L (2016) Biomed Chromatogr 30:2009
9. Brozyna-Heredia IY, Ganoza-Yupanqui ML, Moreno-Exebio L, Dos Santos JL (2022). Crit Rev Anal Chem. https://doi.org/10.1080/10408347.2022.2150071
10. Khan MF, Rita SA, Kayser MS, Islam MS, Asad S, Bin Rashid R, Bari MA, Rahman MM, Al Aman DA, Setu NI (2017) Front Chem 5:27
11. Hartkoorn RC, Khoo S, Back DJ, Tjia JF, Waitt CJ, Chaponda M, Davies G, Ardrey A, Ashleigh S, Ward SA (2007) J Chromatogr B 857:76
12. Ozer T, Henry CS (2024) Curr Top Med Chem 24:952
13. Buledi JA, Shah Z-u-H, Mallah A, Solangi AR (2022) Curr Anal Chem 18:102
14. Kaya SI, Karabulut TC, Kurbanoglu S, Ozkan SA (2020) Current Pharm Anal 16:641
15. Silva RM, da Silva AD, Camargo JR, de Castro BS, Meireles LM, Silva PS, Janegitz BC, Silva TA (2023) Biosensors 13:453
16. Kelíšková P, Matvieiev O, Janíková L, Šelešovská R (2023) Curr Opin Electrochem 42:101408
17. Mohamed HM (2016) Trends Anal Chem 82:1
18. Boumya W, Taoufik N, Achak M, Barka N (2021) J Pharm Anal 11:138
19. Long Y, Zhan Y, Hong S, Mahmud S, Liu H (2024) ChemistrySelect 9:e202303369
20. Farokhi-Fard A, Golichenari B, Mohammadi Ghanbarlou M, Zanganeh S, Vaziri F (2019) Biosens Bioelectron 146:111731
21. AjayI RF, Tshoko S, Mgwili Y, Nqunqa S, Mulaudzi T, Mayedwa N, Iwuoha E (2020) Processes 8:879
22. Torres-Rivero K, Florido A, Bastos-Arrieta J (2021) Sensors 21:2596

23. Cinti S, Arduini F (2017) Biosens Bioelectron 89:107
24. Topal BD, Sener CE, Kaya B, Ozkan SA (2021) Current Pharm Anal 17:421
25. Uwaya GE, Fayemi OE (2022) J Cluster Sci 33:1035
26. Beitollai H, Garkani Nejad F, Tajik S, Jahani S, Biparva P (2017) Int J Nano Dimens 8:197
27. Chen P-Y, Yang H-H, Huang C-C, Chen Y-H, Shih Y (2015) Electrochim Acta 161:100
28. Leonardi SG, Marini S, Espro C, Bonavita A, Galvagno S, Neri G (2017) Microchim Acta 184:2375
29. Dhara K, Stanley J, Ramachandran T, Nair BG, Babu TGS (2016) J Nanosci Nanotechnol 16:8772
30. Tajik S, Beitollahi H, Aflatoonian MR, Mohtat B, Aflatoonian B, Shoaie IS, Khalilzadeh MA, Ziasistani M, Zhang K, Jang HW (2020) RSC Adv 10:15171
31. Dhara K, Thiagarajan R, Nair BG, Thekkedath GSB (2015) Microchim Acta 182:2183
32. Choudhry NA, Kampouris DK, Kadara RO, Jenkinson N, Banks CE (2009) Anal Methods 1:183
33. Liu X-W, Pan P, Zhang Z-M, Guo F, Yang Z-C, Wei J, Wei Z (2016) J Electroanal Chem 763:37
34. Song P, Li Y, Yin S, Tang Y, Wang Z (2021) J Electroanal Chem 901:115784
35. Chakrabarti MH, Low CTJ, Brandon NP, Yufit V, Hashim MA, Irfan MF, Akhtar J, Ruiz-Trejo E, Hussain MA (2013) Electrochim Acta 107:425
36. Gong Z, Zhang G, Wang S (2013) J Chem 2013:756307
37. Alqarni AO, Mahmoud AM, Alyami BA, Ali R, El-Wekil MM (2024) Microchim Acta 191:123
38. Adekunle AS, Ayenimo JG, Fang X-Y, Doherty WO, Arotiba OA, Mamba BB (2011) Int J Electrochem Sci 6:2826
39. Geng B, Yan F, Zhang X, He Y, Zhu C, Chou S-L, Zhang X, Chen Y (2021) Adv Mater 33:2106781
40. Dao X, Nie M, Sun H, Dong W, Xue Z, Li Q, Liao J, Wang X, Zhao X, Yang D, Teng L (2022) Int J Hydrogen Energy 47:16741
41. Kim J, Choi W, Park JW, Kim C, Kim M, Song H (2019) J Am Chem Soc 141:6986
42. Zhang P, Liu H, Li X (2021) Appl Surf Sci 559:149865
43. Zivari-Moshfegh F, Javanmardi F, Nematollahi D (2023) Electrochim Acta 457:142487
44. Alizadeh M, Asrami PN, Altuner EE, Gulbagca F, Tiri RNE, Aygun A, Kaynak İ, Sen F, Cheraghi S (2022) Chemosphere 309:136566
45. González-Sánchez MI, Gómez-Monedero B, Agrisuelas J, Iniesta J, Valero E (2019) J Electroanal Chem 839:75
46. Kozak J, Tyszczuk-Rotko K, Wójciak M, Sowa I, Rotko M (2021) Materials 14:4231
47. Rastgar S, Shahrokhian S (2014) Talanta 119:156
48. Gutiérrez-Fernández S, Blanco-López MC, Lobo-Castañón MJ, Miranda-Ordieres AJ, Tuñón-Blanco P (2004) Electroanalysis 16:1660
49. Alonso Lomillo MA, Domínguez Renedo O, Arcos Martínez MJ (2005) Electrochim Acta 50:1807
50. Tyszczuk K, Korolczuk M (2009) Electroanalysis 21:101
51. Daneshgar P, Norouzi P, Dousty F, Ganjali RM, Moosavi-Movahedi AA (2009) Current Pharm Anal 5:246
52. Asadpour-Zeynali K, Mollarasouli F (2017) Biosens Bioelectron 92:509
53. Amidi S, Ardakani YH, Amiri-Aref M, Ranjbari E, Sepehri Z, Bagheri H (2017) RSC Adv 7:40111
54. Ajayi RF, Sidwaba U, Feleni U, Douman SF, Tovide O, Botha S, Baker P, Fuku XG, Hamid S, Waryo TT, Vilakazi S, Tshihkudo R, Iwuoha EI (2014) Electrochim Acta 128:149
55. Kawde AN, Temerk Y, Farhan N (2014) Acta Chim Slov 61:215–222
56. Shiri S, Pajouheshpoor N, Khoshsafar H, Amidi S, Bagheri H (2017) New J Chem 41:15564
57. Chen T-W, Sivasamy Vasantha A, Chen S-M, Al Farraj DA, Soliman Elshikh M, Alkufeidy RM, Al Khulaifi MM (2019) Ultrason Sonochem 59:104718
58. Santos RHT, Santos NG, Alves JPH, Garcia CAB, Romão LCP, Arguelho MLPM (2008) Bioelectrochemistry 72:122
59. Jin Z, Bard AJ (2020) Proc Natl Acad Sci 117:12651